Journal of Materials Chemistry B

ROYAL SOCIETY OF CHEMISTRY

PAPER

View Article Online
View Journal | View Issue

Check for updates

Cite this: *J. Mater. Chem. B*, 2025, **13**, 14416

Carrier-free single-molecule hypoxia-activated nanoprodrug of SN38 with ultrahigh drug loading for pancreatic cancer treatment

Amrit Regmi, Mouhmad Elayyan, Safiya Nisar and Binglin Sui *

Received 15th June 2025,
Accepted 9th October 2025

DOI: 10.1039/d5tb01434d

rsc.li/materials-b

Pancreatic cancer remains one of the most lethal malignancies for human health. The anticancer drug SN38 has been proven effective against pancreatic cancer cells; however, its clinical application is limited by its poor aqueous solubility and restricted bioavailability *in vivo*. In this work, we developed a novel carrier-free single-molecule hypoxia-responsive nanoprodrug of SN38 for the treatment of pancreatic tumors. The nanoprodrug has an ultrahigh drug-loading content of ~80 wt% and a nanoscale size of ~50 nm. The drug molecules are masked by a hypoxia-sensitive aromatic azo group in the nanoprodrug, thereby shielding the therapeutic effects and toxicities of SN38 under normoxic conditions. Thus, the toxicity of the new regimen toward healthy cells and tissues is alleviated. In response to the upregulated level of azoreductase enzymes in the hypoxic tumor microenvironment, SN38 molecules are released *in situ* with their intact structures, exerting a powerful suppressive effect on tumor cells.

Introduction

To date, continuous efforts have been devoted to seeking more efficient therapeutic strategies to fight against pancreatic cancer in that the 5-year relative survival rate for patients diagnosed with pancreatic cancer has remained the lowest among all types of cancers for a long time.[1,2] The bleak prognosis of the disease necessitates the development of more potent anticancer agents for pancreatic cancer treatment. Irinotecan, a hydrophilic prodrug of SN38 (7-ethyl-10-hydroxycamptothecin), has been approved by the US Food and Drug Administration (FDA) for the treatment of pancreatic cancer.[3] Recent studies revealed that only a small amount (2–8%) of irinotecan is converted to SN38 *in vivo*.[4,5] SN38 is a potent topoisomerase I inhibitor that has demonstrated effective antitumor activity, 100–1000 times more active than irinotecan.[6] However, the clinical application of SN38 is severely limited by its poor aqueous solubility, instability under physiological conditions, and nonselective biodistribution in the body.[7] These challenges have spurred interest in prodrug strategies aimed at enhancing the pharmacokinetic profile, tumor selectivity, and therapeutic efficacy of SN38.[8] Hence, therapeutic regimens with higher efficiency to improve the bioavailability and therapeutic efficacy of SN38 are still in need.

Hypoxia, a condition of insufficient oxygen supply, is a key feature of the tumor microenvironment involved in the pathogenesis of pancreatic ductal adenocarcinoma (PDAC), which is the most common type of pancreatic cancer, accounting for more than 90% of pancreatic cancer cases.[9] As solid tumors rapidly proliferate, their oxygen demand often surpasses the capacity of the surrounding abnormal vasculature, resulting in regions of low oxygen tension.[10,11] The hypoxic microenvironment contributes not only to cancer cell survival and metabolic reprogramming but also to immune evasion and resistance to radiotherapy and chemotherapy.[12] Hypoxia activates a cascade of molecular pathways, most notably those mediated by hypoxia-inducible factors (HIFs), which regulate the expression of genes involved in angiogenesis, glycolysis, and cell survival.[13,14] This adaptation supports tumor growth under harsh conditions and promotes a more aggressive phenotype. Given its multifaceted role, hypoxia presents both a challenge and an opportunity in cancer therapy. On one hand, it contributes to poor prognosis and limits the effectiveness of standard treatments. On the other hand, it offers a unique target for therapeutic intervention. Recent advances in hypoxia-targeted therapies, including hypoxia-activated prodrugs and hypoxia-responsive nanomedicines,[15–19] have opened new avenues for more effective and selective cancer treatments. Hypoxia-activated therapeutic prodrugs of SN38 have also been designed to improve its therapeutic efficiency,[20–22] among which Kim *et al.* developed an aromatic azo-based SN38 prodrug for theranostic tumor imaging and therapy.[23]

Herein, we present a carrier-free single-molecule nanoprodrug (NPD) of SN38, denoted as SN38-Azo1-NPD, with ultrahigh

Department of Chemistry, University of North Dakota, Grand Forks, North Dakota 58202, USA. E-mail: binglin.sui@und.edu

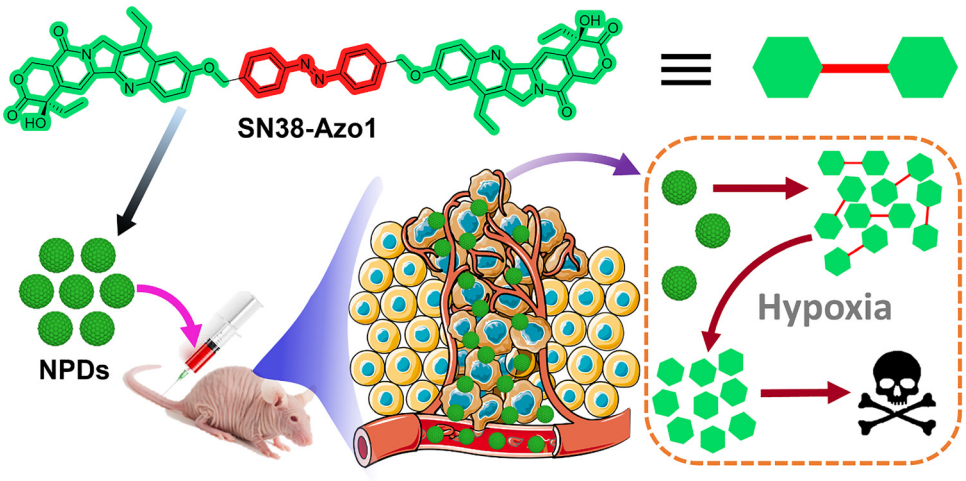

Scheme 1 Schematic illustration of the fabrication of SN38-Azo1-NPD, tumor accumulation, and hypoxia-triggered intracellular drug release. The SN38-Azo1 prodrug molecule contains two molecular units of SN38 linked by a hypoxia-responsive self-immolating azo-containing group (Ph–N═N–Ph, in red). The NPDs are constructed through a nano-assembling process upon dispersion into aqueous media. When being injected into the body, they accumulate at tumor sites *via* the EPR effect. Upon entering cancer cells, the NPDs disassemble into SN38-Azo1 molecules, which are subsequently converted to SN38 molecules through the self-immolation of the azo-containing drug linker triggered by the hypoxic condition.

drug loading for the high-efficiency treatment of pancreatic tumors. The NPD is composed of a new dimeric prodrug (SN38-Azo1), which can be activated by the hypoxic tumor microenvironment to release SN38 drug molecules. As illustrated in Scheme 1, the prodrug molecule contains two molecular units of SN38 linked by a self-immolating azo-benzene (Ph–N═N–Ph) group. Thus, the drug molecules are masked by the drug linker, and their biological functions are confined by the NPD formulation. As known, azoreductase enzymes are upregulated in hypoxic tumor cells.[24–26] Under deficient oxygen conditions, they catalyze the reduction and subsequent cleavage of the azo bond, which has been explored for hypoxia-leveraged tumor diagnosis and therapeutics.[27–29] Thereby, upon self-delivering into tumor tissues and cancer cells, the NPDs disassemble into hypoxia-responsive SN38-Azo1 molecules, which subsequently are converted to SN38 molecules by the azoreductase enzymes in the tumor microenvironment. Meanwhile, the accumulation of drug molecules in tumors is elevated by the NPD formulation due to the enhanced permeability and retention (EPR) effect.[30,31] The combination of enhanced tumor accumulation and tumor microenvironment-activated drug release results in improved therapeutic efficacy against tumors and reduced toxicity toward normal tissues.

The hypoxia-sensitive drug linker contained in the NPD was synthesized within two steps. As shown in Scheme 2, a commercial chemical, 4-nitrobenzyl alcohol, was used to synthesize compound **1**, 1,2-bis(4-(hydroxymethyl)phenyl)diazene, with zinc powder as the reducing agent. Upon reacting with thionyl chloride, the hydroxyl groups of **1** were turned into chlorine atoms, producing compound **2**, 1,2-bis(4-(chloromethyl)phenyl)diazene. The chemical structures of the intermediates were confirmed by NMR spectroscopy (Fig. S1–S4). The prodrug SN38-Azo1 was obtained through the replacement of chlorine atoms of compound **2** by SN38 molecules, and its chemical structure was characterized by ^{1}H NMR (Fig. S5), ^{13}C NMR (Fig. S6), and HRMS (Fig. S7).

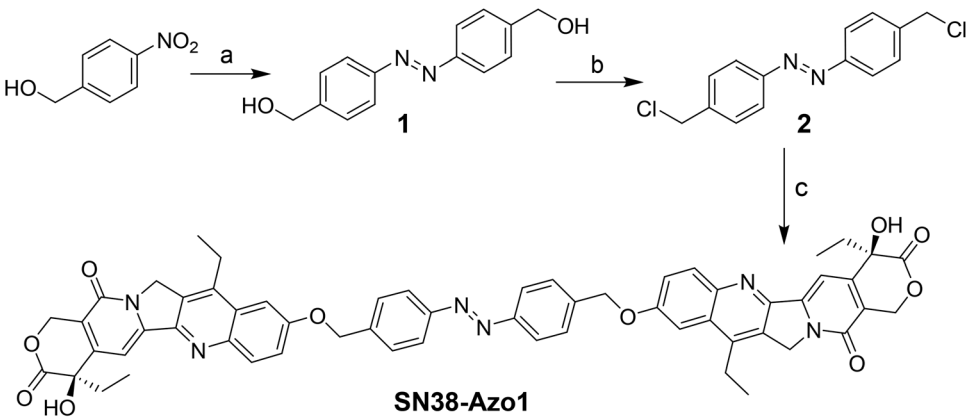

Scheme 2 Synthesis of SN38-Azo1. Reaction conditions: (a) Zn (powder), NaOH (20% in water), 70 °C; (b) $SOCl_2$, DCM, room temperature; (c) SN38, K_2CO_3, DMF, 80 °C.

To optimize the accumulation and retention of the drug in tumor tissues and cells, we constructed SN38-Azo1 into a nanoprodrug (SN38-Azo1-NPD) to take advantage of the EPR effect of nanoscale particles. SN38-Azo1-NPD was formulated according to an established nano-assembling protocol.[32] As depicted in Fig. 1A, upon being dispersed into an aqueous medium, the dimeric prodrug molecules self-assemble into nanoparticles due to intermolecular π–π stacking, hydrophobic interaction, and hydrogen bonding.[33–35] The resulting NPDs were characterized by dynamic light scattering (DLS) and transmission electron microscopy (TEM). DLS analysis revealed that SN38-Azo1-NPD had a diameter of 54.1 nm with a polydispersity index (PDI) value of 0.17 (Fig. 1B). A negative surface charge was also detected (zeta potential: −13.5 mV). TEM images of the nanostructures displayed a spherical morphology and a dry-state diameter of ∼50 nm (Fig. 1C). These data signified the desired dimensions of SN38-Azo1-NPD for *in vivo* tumor treatment because nanoparticles with a size of 5–50 nm are more efficacious in entering tumor tissues and cancer cells, while those in the range of 50–200 nm have a tendency to circulate longer in the bloodstream and retain more in tumor tissues.[36–38] The drug loading efficiency during the nano-assembling process was measured to be 87%. Noteworthily, SN38-Azo1-NPD has an exceedingly high drug-loading content (79.2%) compared to that of reported SN38-delivering systems (generally < 35%).[39–44]

In order to elucidate the molecular stacking pattern and driving force for the assembly of the single-molecule NPD, we conducted theoretical modeling based on density functional theory (DFT) calculations using the Gaussian 16 software suite. The Becke 3-parameter Lee–Yang–Parr (B3LYP) functional was employed for the modeling calculations due to its excellence in predicting properties of organic compounds.[45,46] Dispersion corrections, specifically D3 dispersion of Grimme's Dispersion with Beck–Johnson damping (GD3BJ), were used alongside the B3LYP functional.[47,48] Meanwhile, the calculations used the Pople Basis, 6-31G(d,p), which is comprised of 6 primitive gaussians for core orbitals, split valence double zeta basis and polarization functions on heavy (d) and hydrogen (p) atoms.[49,50] Using the B3LYP-GD3BJ/6-31G(d,p) method, we studied the relationship between the potential energy and the distance between two SN38-Azo1 molecules during the molecular stacking process. The two molecules are in overlap positions with each other as they stack (Fig. 2A). As shown in Fig. 2B, the potential energy decreases gradually as the distance between the molecules becomes shorter, reaching a minimum at a distance of 3.4 Å. A further shorter distance increases the potential energy. These results demonstrate that 3.4 Å is an optimal distance for the stacking of SN38-Azo1 molecules, and the minimum potential energy serves as the driving force for this process. The data also support a π–π stacking pattern for the assembly of the single-molecule NPD, as the typical distance of π–π stacking is from 3.2–3.7 Å.[51,52]

The hydrodynamic stability of SN38-Azo1-NPD was studied in diverse aqueous media. No significant change was observed in its hydrodynamic size when dispersed in deionized water over a period of two months (Fig. S8), which indicated the long-term storage stability of the NPDs. To assess the stability under different biological conditions, the NPDs were dispersed in PBS buffer (pH 7.4) solutions with and without fetal bovine serum (FBS). As shown in Fig. 3A, SN38-Azo1-NPD exhibited high colloidal stability in PBS buffer, and its stability was unaffected by the presence of FBS, as indicated by the barely altered hydrodynamic diameter of the NPDs, which suggests its suitability for *in vivo* applications in biological environments.

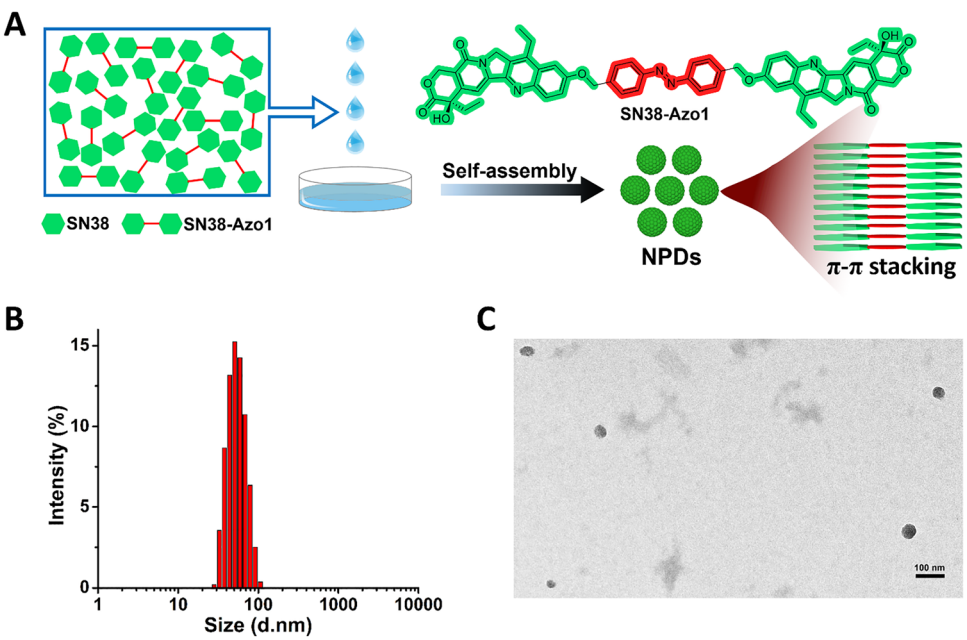

Fig. 1 (A) Schematic illustration of the fabrication of SN38-Azo1-NPD *via* a nano-assembling procedure. Upon dispersion into aqueous media, SN38-Azo1 molecules spontaneously assemble into nanoparticles, driven by π–π stacking. (B) Size distribution and (C) TEM image of SN38-Azo1-NPD.

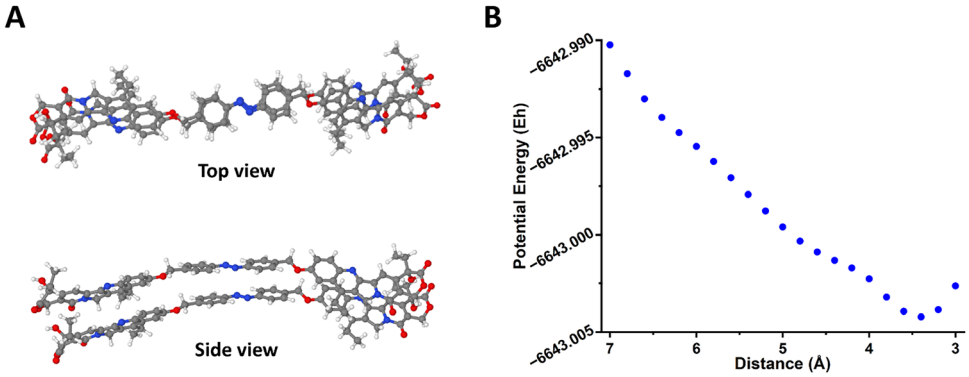

Fig. 2 (A) Top and side views of SN38-Azo1 molecules during the molecular stacking process. (B) The correlation between the potential energy and the distance between two stacking molecules.

The stimulus-responsive drug release profiles of SN38-Azo1-NPD were also studied in degassed PBS buffer solutions. Different biological species were added to serve as possible stimuli for triggering the release of SN38 molecules. Rat liver microsome (RLM) and reduced nicotinamide adenine dinucleotide phosphate (NADPH) were used as a source of the azoreductase enzyme and the electron source to reduce the aromatic azo groups, respectively.[53] As shown in Fig. 3B, the addition of FBS (10%), NADPH (1 mM), RLM (100 μg mL^{-1}), or the combinations FBS + NADPH and FBS + RLM was not able to trigger the release of SN38. However, in the presence of NADPH + RLM, the drug release was successfully activated, leading to approximately 90% of the drug released within 24 h, and furthermore, the coexistence of FBS induced no considerable impact on the drug release efficiency. In addition, the release rate of SN38 was dependent on the concentration of the enzyme, as evidenced by the accelerated drug release in the presence of higher enzyme levels (Fig. 3C). These findings inferred that the azo bond of SN38-Azo1 can be reduced in the presence of azoreductase enzyme with NADPH as the electron source, resulting in the release of SN38 molecules. As illustrated in Fig. 3D, upon receiving electrons from NADPH, the azo bond in the prodrug is cleaved by the reduction, being converted into two amino groups. Thereby, the SN38-Azo1 molecule is split into two equal halves. The resulting molecular segments contain a 4-methylene aniline group, which is unstable and immediately self-eliminates to form a stable molecule, 4-methylenecyclohexa-2,5-dienimine, simultaneously converting the prodrug half into an intact SN38 molecule. The traceless release of SN38 was validated by HRMS analysis of the resultant species in the final drug-release solutions, which corroborated the plausibility of the mechanism.

In order to assess the suitability of SN38-Azo1-NPD for cellular uptake examination, we measured its photophysical properties using UV-vis spectroscopy and fluorescence spectroscopy. As shown in Fig. 4A, an absorption peak at 370 nm and a fluorescence emission peak at 426 nm were observed. The uptake of SN38-Azo1-NPD by cancer cells was examined by

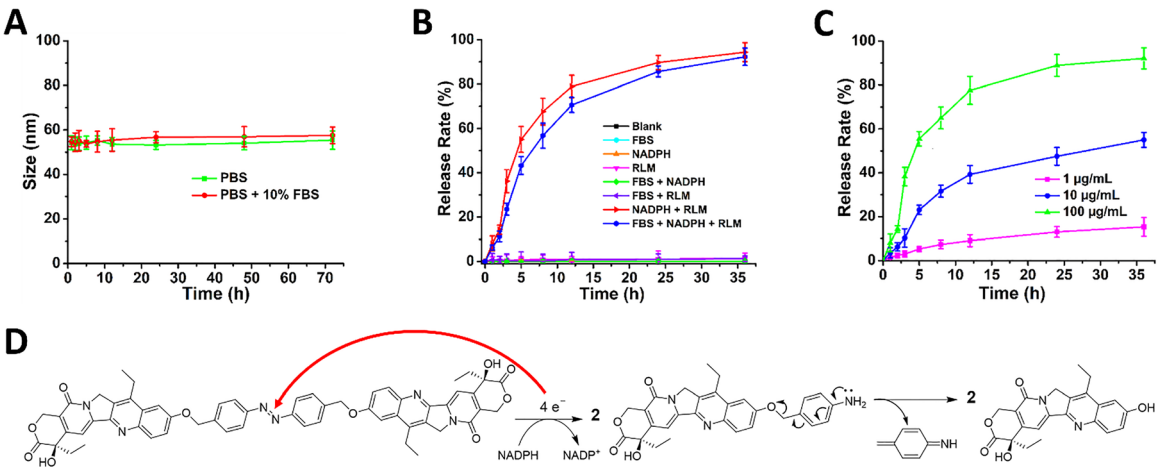

Fig. 3 (A) Hydrodynamic stability of SN38-Azo1-NPD in PBS (pH 7.4) and PBS + 10% FBS solutions. (B) Drug release profiles of SN38-Azo1-NPD in PBS (blank) containing FBS (10%), NADPH (1 mM), RLM (100 μg mL^{-1}), FBS (10%) + NADPH (1 mM), FBS (10%) + RLM (100 μg mL^{-1}), NADPH (1 mM) + RLM (100 μg mL^{-1}), and FBS (10%) + NADPH (1 mM) + RLM (100 μg mL^{-1}). (C) Stimulus-responsive release profiles of SN38-Azo1-NPD in PBS containing NADPH (1 mM) and varied concentrations of RLM (1, 10, and 100 μg mL^{-1}). (D) Mechanism of the enzyme-activated traceless release of SN38. Data represent the means ± SD, n = 3.

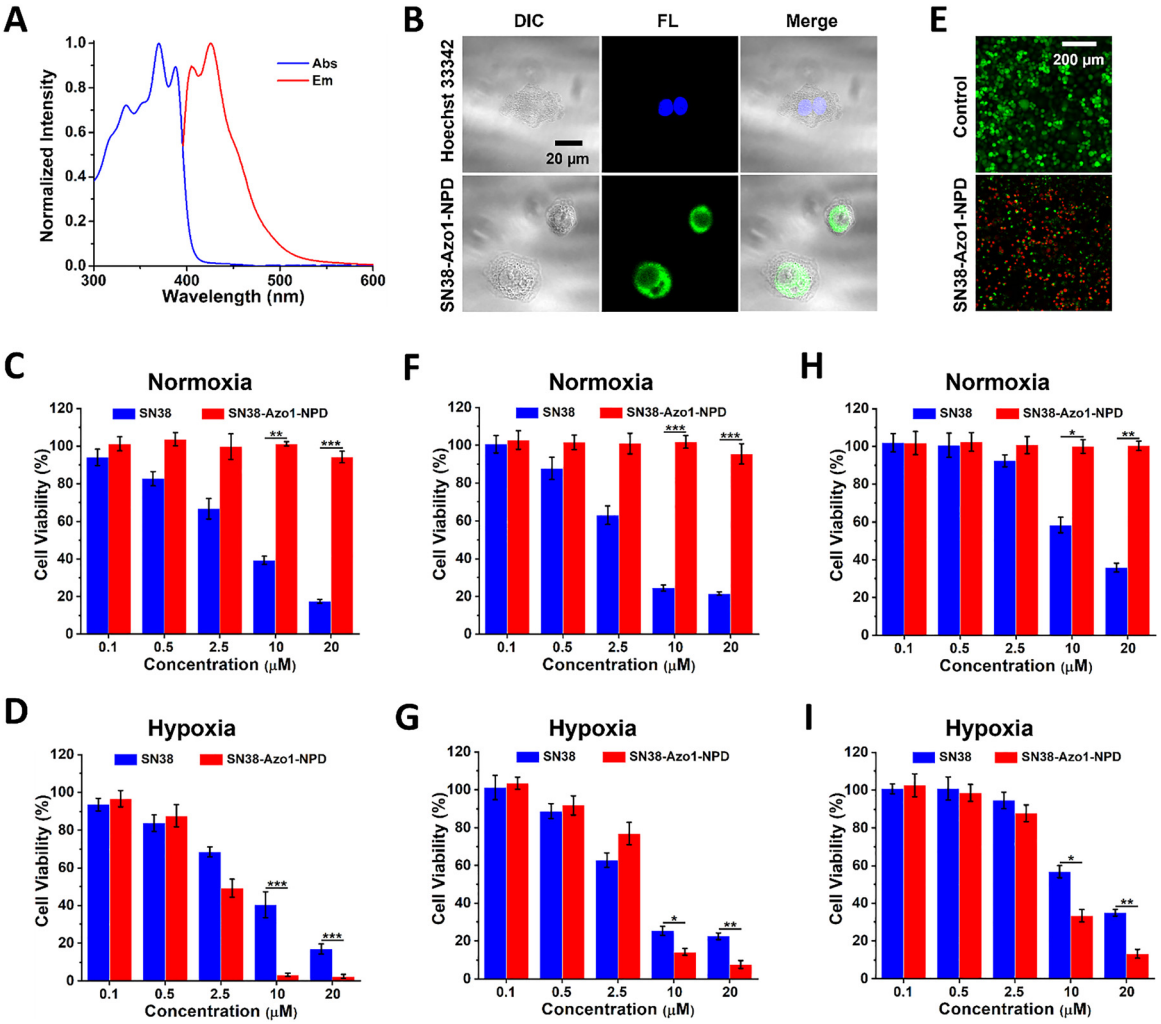

Fig. 4 (A) UV-vis absorption and fluorescence emission spectra of SN38-Azo1-NPD. (B) CLSM images of BxPC-3 cells after incubation with Hoechst 33342 (blue) and SN38-Azo1-NPD (green) for 1 h. Cell viability of BxPC-3 cells treated with varied concentrations of SN38 and SN38-Azo1-NPD under (C) normoxic and (D) hypoxic conditions. (E) Fluorescence images of BxPC-3 cells stained with calcein AM (green) and PI (red) after treatment with SN38-Azo1-NPD under hypoxic conditions. Cell viability of AsPC-1 (F) and (G) and PANC-1 (H) and (I) cells treated with varied concentrations of SN38 and SN38-Azo1-NPD under normoxic (F) and (H) and hypoxic (G) and (I) conditions. Data represent the means ± SD, $n = 3$. *$P < 0.05$; **$P < 0.01$; and ***$P < 0.001$.

confocal laser scanning microscopy (CLSM) in human pancreatic cancer BxPC-3 cells. As shown in Fig. 4B, cells emitted striking fluorescence after incubation with SN38-Azo1-NPD, which confirmed that the NPDs effectively self-delivered into cancer cells.

Next, the *in vitro* cytotoxicity of SN38-Azo1-NPD was evaluated by the 3-(4,5-dimethylthiazol-2-yl)-2,5-diphenyl tetrazolium bromide (MTT) assay. The viability of BxPC-3 cancer cells was measured after they were incubated with free SN38 drug and SN38-Azo1-NPD at different concentrations (0–20 μM) for 24 h. To reveal the hypoxia activation of the NPD, the MTT assays were carried out under hypoxic conditions (1% O_2 + 94% N_2 + 5% CO_2). Prior to the treatment period, cells were cultured under a low-oxygen condition (1% O_2) for 6 h to generate a hypoxic intracellular environment with enhanced levels of azoreductase enzymes, mimicking the hypoxic microenvironment of solid tumors. Meanwhile, MTT assays under normoxic conditions (20% O_2 + 75% N_2 + 5% CO_2) were conducted as a control. Under normoxic conditions, SN38 exerted a dose-dependent inhibitory effect on the proliferation of cells, indicating the anticancer potency of the drug against cancer cells, whereas SN38-Azo1-NPD induced little to no cytotoxicity toward cells (Fig. 4C). In contrast, in the presence of hypoxia, the NPD imposed an overwhelming anticancer effect on cell proliferation, which was more potent than that generated by SN38, while the latter maintained the same level of suppression on cell growth as under normoxic conditions (Fig. 4D). The drastic differences in the cell-killing activities of the two treatments under normoxic and hypoxic conditions demonstrated that the NPD formulation effectively masked the cytotoxicity of SN38, resulting in the negligible therapeutic effect of SN38-Azo1-NPD under normoxia, and released the bioactive SN38 drug molecules with high efficiency, triggered by the elevated level of azoreductase enzymes under hypoxia. Additionally, the cell apoptosis induced by SN38-Azo1-NPD was investigated using live & dead cell staining, where live and dead cells were stained with Calcein-AM and

PI, respectively. As shown in Fig. 4E a significant number of cells were undergoing apoptosis after treatment with SN38-Azo1-NPD under hypoxic conditions. To further verify the therapeutic efficiency of the treatments, we performed the same *in vitro* cytotoxicity tests in other pancreatic cancer cells. As a result, similar behaviors of the SN38 drug and SN38-Azo1-NPD also occurred under respective normoxic and hypoxic conditions in AsPC-1 (Fig. 4F and G) and PANC-1 (Fig. 4H and I) cells. These findings suggest that the NPD technique holds great potential for killing tumor cells while causing reduced damage to normal cells due to the absence of a hypoxic microenvironment.

Encouraged by the promising performances of the NPD in the *in vitro* experiments, we further studied SN38-Azo1-NPD in a xenograft BxPC-3 tumor model established in mice. To validate our hypothesis that the NPD could deliver themselves into tumor tissues due to the EPR effect, we examined the *in vivo* biodistribution of SN38-Azo1-NPD in pancreatic tumor-bearing mice by a Lago X animal imaging system. Mice were intravenously injected with SN38-Azo1-NPD dispersed in sterilized PBS at a dose of 1 mg kg^{-1}. After 6 h post-injection, the mice were euthanized, and their major organs, including the heart, liver, spleen, lungs, and kidneys, and tumor tissues were excised for *ex vivo* imaging to assess the biodistribution of the NPD in various tissues. As shown in Fig. 5A, intense fluorescence emission signals were detected in the tumors of mice. The related quantitative analysis showed that the fluorescence intensity of tumors was significantly higher than that of other organs (Fig. 5B), confirming the enhanced accumulation and retention of SN38-Azo1-NPD in tumor tissues.

Further, we investigated the *in vivo* therapeutic efficacy of the NPD in combating pancreatic tumors. As depicted in Fig. 5C, the entire experiment lasted 5 weeks, from tumor inoculation to the administration of drug/NPD and the termination of the experiment. Mice bearing BxPC-3 tumors were randomly divided into three groups and intravenously administered with different treatments, including PBS (the control group), free SN38 drug, and SN38-Azo1-NPD. The administrations were repeated twice per week for three weeks. Fig. 5D illustrates the changes in tumor volume of mice following various treatments. In the control group, tumors grew rapidly in an unrestricted manner, and the relative tumor volume reached nearly 14-fold after three weeks. Free SN38 moderately impeded tumor growth, and the tumor volume was approximately 6 times larger by the end of treatment. In stark contrast

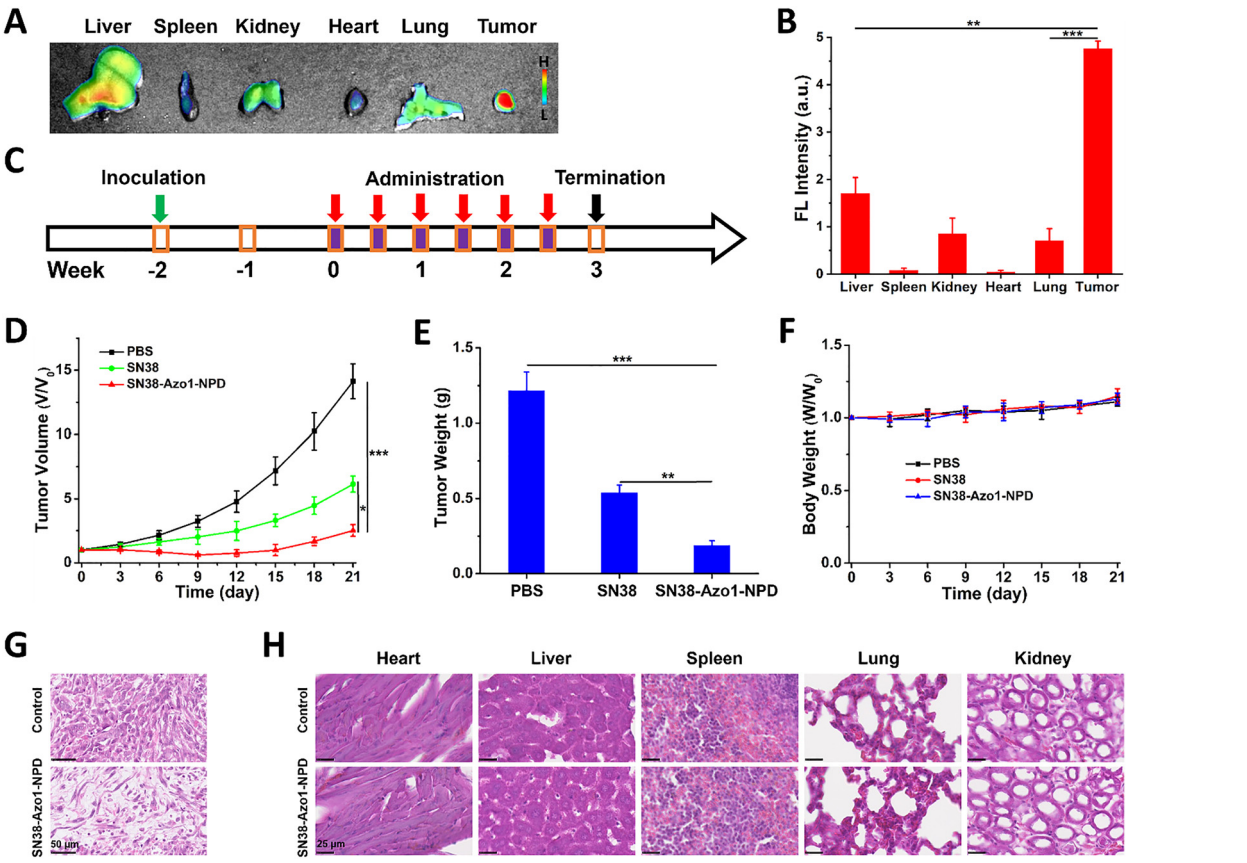

Fig. 5 *In vivo* biodistribution and therapeutic efficacy of SN38-Azo1-NPD in a xenograft pancreatic tumor model in mouse. (A) *Ex vivo* images and (B) the corresponding average fluorescence intensity of organs and tumors of mice after treatments with SN38-Azo1-NPD. (C) Treatment timeline for the tumor treatment. (D) Relative tumor volume of mice with varied treatments. (E) The weight of tumors harvested from sacrificed mice in different treatment groups. (F) Changes in the body weight of mice over time. H&E staining images of (G) tumors and (H) mice organs after different treatments. Data represent the means ± SD, $n = 5$. *$P < 0.05$; **$P < 0.01$; and ***$P < 0.001$.

to those, the SN38-Azo1-NPD administration imposed a powerful inhibition on the growth of tumors. The tumor burdens in mice gradually shrank at the beginning of the treatment, and a relative tumor volume of ~2.4-fold was found at the end of the experiment. These results were further validated by the analytical statistics of tumor solids collected from sacrificed mice. As shown in Fig. 5E, the average tumor weight of mice administrated with SN38-Azo1-NPD was significantly smaller than that of mice in the other groups, suggesting that the tumor growth was efficaciously suppressed by the NPD treatment. Additionally, no considerable loss in body weight was observed in mice after these treatments, indicating that the treatments brought no severe systemic toxicities to mice (Fig. 5F). Histological examination of the dissected tumors collected from sacrificed mice using hematoxylin and eosin (H&E) staining revealed that in mice treated with SN38-Azo1-NPD, tumor cells exhibited significant cell death, and cell proliferation was substantially suppressed in comparison to those in the control group (Fig. 5G). These findings further validated the efficacious hypoxia-responsive drug release of the NPDs in the hypoxic tumor microenvironment. Moreover, no apparent histological damage was observed in the H&E-stained tissue sections of major organs excised from euthanized mice at the end of the experiment (Fig. 5H), which, in combination with the potent tumor inhibitory effects of SN38-Azo1-NPD, signified the potential of the NPD formulation for treating pancreatic cancer.

Conclusion

A carrier-free single-molecule hypoxia-activated nanoprodrug, SN38-Azo1-NPD, based on the anticancer drug SN38, has been developed for high-efficiency treatment of pancreatic cancer *in vivo*. A new SN38 prodrug, SN38-Azo1, consisting of two molecular units of SN38 and a self-immolating azo-benzene group, was synthesized *via* three straightforward reactions. The prodrug was assembled into uniform nanostructures approximately 50 nm in diameter, exhibiting excellent hydrodynamic stability through a simple one-step nanoprecipitation protocol. SN38-Azo1-NPD has an ultrahigh drug-loading content due to the carrier-free single-molecule formulation. It displayed a dose-dependent response to azoreductase enzymes in the presence of NADPH, leading to the traceless release of SN38 molecules by means of the self-immolation of the azo-based drug linker. Thanks to the inherent fluorescence emission, *in vitro* cellular uptake of SN38-Azo1-NPD manifested effective intracellular drug delivery. MTT assays in pancreatic cancer cells revealed that the nanoformulation technique effectively masked the cytotoxicity of SN38 under normoxic conditions and generated a desired therapeutic effect against cancer cells under hypoxic conditions, owing to the hypoxia-activated drug release. The *in vivo* biodistribution results confirmed the enhanced accumulation and retention of the NPD in tumor tissues, which benefited from its optimal nanoscale dimension. Finally, SN38-Azo1-NPD demonstrated potent antitumor efficacy, significantly more efficient than SN38, in treating pancreatic tumors in mice, devoid of causing additional systemic toxicities, thus overcoming the drawbacks of the free drug. The research outcomes suggest that the new regimen of SN38 may have translational value for the clinical treatment of pancreatic cancer.

Conflicts of interest

The authors declare no competing financial interest.

Data availability

The data supporting this article have been included as part of the supplementary information (SI). Supplementary information: Detailed experimental conditions and methods; Fig. S1–S8. See DOI: **https://doi.org/10.1039/d5tb01434d**.

Acknowledgements

We acknowledge the funding support of the National Science Foundation (CHE-2213445). We also acknowledge the UND Behavioral Research Core Facility for animal studies.

References

1 R. L. Siegel, A. N. Giaquinto and A. Jemal, *Cancer J. Clin.*, 2024, **74**(1), 12–49.
2 C. J. Halbrook, C. A. Lyssiotis, M. Pasca di Magliano and A. Maitra, Pancreatic cancer: Advances and challenges, *Cell*, 2023, **186**(8), 1729–1754.
3 M. B. Brown and H. A. Blair, Liposomal Irinotecan: A Review as First-Line Therapy in Metastatic Pancreatic Adenocarcinoma, *Drugs*, 2025, **85**(2), 255–262.
4 J. Si, X. Zhao, S. Gao, D. Huang and M. Sui, Advances in delivery of Irinotecan (CPT-11) active metabolite 7-ethyl-10-hydroxycamptothecin, *Int. J. Pharm.*, 2019, **568**, 118499.
5 M. Kciuk, B. Marciniak and R. Kontek, Irinotecan—Still an Important Player in Cancer Chemotherapy: A Comprehensive Overview, *Int. J. Mol. Sci.*, 2020, **21**(14), 4919.
6 V. Bala, S. Rao, B. J. Boyd and C. A. Prestidge, Prodrug and nanomedicine approaches for the delivery of the camptothecin analogue SN38, *J. Controlled Release*, 2013, **172**(1), 48–61.
7 Y. Matsumura, Preclinical and clinical studies of NK012, an SN-38-incorporating polymeric micelles, which is designed based on EPR effect, *Adv. Drug Delivery Rev.*, 2011, **63**(3), 184–192.
8 Y. Dai, M. Qian and Y. Li, Structural Modification Endows Small-Molecular SN38 Derivatives with Multifaceted Functions, *Molecules*, 2023, **28**(13), 4931.
9 M. Orth, P. Metzger, S. Gerum, J. Mayerle, G. Schneider, C. Belka, M. Schnurr and K. Lauber, Pancreatic ductal adenocarcinoma: biological hallmarks, current status, and future perspectives of combined modality treatment approaches, *Radiat. Oncol.*, 2019, **14**(1), 141.

10 A. L. Harris, Hypoxia—a key regulatory factor in tumour growth, *Nat. Rev. Cancer*, 2002, **2**(1), 38–47.
11 J. A. Bertout, S. A. Patel and M. C. Simon, The impact of O2 availability on human cancer, *Nat. Rev. Cancer*, 2008, **8**(12), 967–975.
12 C.-C. Huang, W.-T. Chia, M.-F. Chung, K.-J. Lin, C.-W. Hsiao, C. Jin, W.-H. Lim, C.-C. Chen and H.-W. Sung, An Implantable Depot That Can Generate Oxygen in Situ for Overcoming Hypoxia-Induced Resistance to Anticancer Drugs in Chemotherapy, *J. Am. Chem. Soc.*, 2016, **138**(16), 5222–5225.
13 Y. Ye, Q. Hu, H. Chen, K. Liang, Y. Yuan, Y. Xiang, H. Ruan, Z. Zhang, A. Song, H. Zhang, L. Liu, L. Diao, Y. Lou, B. Zhou, L. Wang, S. Zhou, J. Gao, E. Jonasch, S. H. Lin, Y. Xia, C. Lin, L. Yang, G. B. Mills, H. Liang and L. Han, Characterization of hypoxia-associated molecular features to aid hypoxia-targeted therapy, *Nat. Metab.*, 2019, **1**(4), 431–444.
14 W. H. Chang and A. G. Lai, The hypoxic tumour microenvironment: A safe haven for immunosuppressive cells and a therapeutic barrier to overcome, *Cancer Lett.*, 2020, **487**, 34–44.
15 Y. Pan, L. Liu, X. Mou and Y. Cai, Nanomedicine Strategies in Conquering and Utilizing the Cancer Hypoxia Environment, *ACS Nano*, 2023, **17**(21), 20875–20924.
16 J. George Joy, G. Sharma and J.-C. Kim, Tailoring polymeric nanocarriers for hypoxia-specific drug release: Insights into design and applications in clinics, *Chem. Eng. J.*, 2024, **496**, 153978.
17 M. H. C. Boulet, H. R. Bolland, E. M. Hammond and A. C. Sedgwick, Oxali(IV)Fluors: Fluorescence Responsive Oxaliplatin(IV) Complexes Identify a Hypoxia-Dependent Reduction in Cancer Cells, *J. Am. Chem. Soc.*, 2023, **145**(24), 12998–13002.
18 S. Nisar and B. Sui, A nitroreductase-sensitive near-IR fluorescent biosensor for detecting tumor hypoxia in vivo, *Sens. Diagn.*, 2024, **3**(9), 1505–1512.
19 J. Zhang, X.-W. Han, P. Chen, G.-G. Shan, G. Jin, H.-T. Feng and B. Z. Tang, Photodynamic Therapy-Accelerated Hypoxia-Responsive Prodrug Release for Synergistic Photo-Chemotherapy of Melanoma Cancer Based on Noncovalent Interactions, *ACS Mater. Lett.*, 2025, **7**(3), 770–779.
20 R. Kumar, E.-J. Kim, J. Han, H. Lee, W. S. Shin, H. M. Kim, S. Bhuniya, J. S. Kim and K. S. Hong, Hypoxia-directed and activated theranostic agent: Imaging and treatment of solid tumor, *Biomaterials*, 2016, **104**, 119–128.
21 C. Jin, Q. Zhang and W. Lu, Synthesis and biological evaluation of hypoxia-activated prodrugs of SN-38, *Eur. J. Med. Chem.*, 2017, **132**, 135–141.
22 S.-Y. Yao, A.-K. Ying, Z.-T. Jiang, Y.-Q. Cheng, W.-C. Geng, X.-Y. Hu, K. Cai and D.-S. Guo, Single Molecular Nanomedicines Based on Macrocyclic Carrier-Drug Conjugates for Concentration-Independent Encapsulation and Precise Activation of Drugs, *J. Am. Chem. Soc.*, 2024, **146**(20), 14203–14212.
23 Y. Zhou, M. Maiti, A. Sharma, M. Won, L. Yu, L. X. Miao, J. Shin, A. Podder, K. N. Bobba, J. Han, S. Bhuniya and J. S. Kim, Azo-based small molecular hypoxia responsive theranostic for tumor-specific imaging and therapy, *J. Controlled Release*, 2018, **288**, 14–22.
24 J. Mei and H. Tian, Most recent advances on enzyme-activatable optical probes for bioimaging, *Aggregate*, 2021, **2**(2), e32.
25 R. Kumari, D. Sunil, R. S. Ningthoujam and N. V. A. Kumar, Azodyes as markers for tumor hypoxia imaging and therapy: An up-to-date review, *Chem.-Biol. Interact.*, 2019, **307**, 91–104.
26 W. Piao, S. Tsuda, Y. Tanaka, S. Maeda, F. Liu, S. Takahashi, Y. Kushida, T. Komatsu, T. Ueno, T. Terai, T. Nakazawa, M. Uchiyama, K. Morokuma, T. Nagano and K. Hanaoka, Development of Azo-Based Fluorescent Probes to Detect Different Levels of Hypoxia, *Angew. Chem., Int. Ed.*, 2013, **52**(49), 13028–13032.
27 J. Xiong, P. Wang, S. Son, C. Zhong, F. Zhang, Z. Mao, Z. Liu and J. S. Kim, Engineering a theranostic platform for synergistic hypoxia-responsive photodynamic therapy and chemotherapy, *Matter*, 2022, **5**(5), 1502–1519.
28 W.-C. Geng, S. Jia, Z. Zheng, Z. Li, D. Ding and D.-S. Guo, A Noncovalent Fluorescence Turn-on Strategy for Hypoxia Imaging, *Angew. Chem., Int. Ed.*, 2019, **58**(8), 2377–2381.
29 S. Guisán-Ceinos, A. Rivero, F. Romeo-Gella, S. Simón-Fuente, S. Gómez-Pastor, N. Calvo, A. Orrego, M. Guisán, I. Corral, F. Sanz-Rodriguez and M. Ribagorda, Turn-on Fluorescent Biosensors for Imaging Hypoxia-like Conditions in Living Cells, *J. Am. Chem. Soc.*, 2022, **144**(18), 8185–8193.
30 H. Maeda, H. Nakamura and J. Fang, The EPR Effect for Macromolecular Drug Delivery to Solid Tumors: Improvement of Tumor Uptake, Lowering of Systemic Toxicity, and Distinct Tumor Imaging In Vivo, *Adv. Drug Delivery Rev.*, 2013, **65**(1), 71–79.
31 Y. Min, J. M. Caster, M. J. Eblan and A. Z. Wang, Clinical Translation of Nanomedicine, *Chem. Rev.*, 2015, **115**(19), 11147–11190.
32 S. Nisar, E. Starosta, M. Elayyan, A. Regmi and B. Sui, Photoinduced Electron Transfer-Based Glutathione-Sensing Theranostic Nanoprodrug with Self-Tracking and Real-Time Drug Release Monitoring for Cancer Treatment, *ACS Appl. Mater. Interfaces*, 2024, **16**(6), 6859–6867.
33 B. Sun, C. Luo, H. Yu, X. Zhang, Q. Chen, W. Yang, M. Wang, Q. Kan, H. Zhang, Y. Wang, Z. He and J. Sun, Disulfide Bond-Driven Oxidation- and Reduction-Responsive Prodrug Nanoassemblies for Cancer Therapy, *Nano Lett.*, 2018, **18**(6), 3643–3650.
34 D. Hao, Q. Meng, B. Jiang, S. Lu, X. Xiang, Q. Pei, H. Yu, X. Jing and Z. Xie, Hypoxia-Activated PEGylated Paclitaxel Prodrug Nanoparticles for Potentiated Chemotherapy, *ACS Nano*, 2022, **16**(9), 14693–14702.
35 L. Guanting, J. Qianhui, X. Fengli, F. Shuwen, Z. Xuanbo, X. Hongying, T. Chutong, L. Qingzhi, S. Jin, H. Zhonggui and S. Bingjun, Smart stimuli-responsive carrier-free nanoassembly of SN38 prodrug as efficient chemotherapeutic nanomedicine, *Acta Mater. Med.*, 2023, **2**(1), 54–63.

36 L. Tang, X. Yang, Q. Yin, K. Cai, H. Wang, I. Chaudhury, C. Yao, Q. Zhou, M. Kwon, J. A. Hartman, I. T. Dobrucki, L. W. Dobrucki, L. B. Borst, S. Lezmi, W. G. Helferich, A. L. Ferguson, T. M. Fan and J. Cheng, Investigating the optimal size of anticancer nanomedicine, *Proc. Natl. Acad. Sci. U. S. A.*, 2014, **111**(43), 15344–15349.

37 J. Xu, M. Song, Z. Fang, L. Zheng, X. Huang and K. Liu, Applications and challenges of ultra-small particle size nanoparticles in tumor therapy, *J. Controlled Release*, 2023, **353**, 699–712.

38 Y. Niu, J. Zhu, Y. Li, H. Shi, Y. Gong, R. Li, Q. Huo, T. Ma and Y. Liu, Size shrinkable drug delivery nanosystems and priming the tumor microenvironment for deep intratumoral penetration of nanoparticles, *J. Controlled Release*, 2018, **277**, 35–47.

39 J. Wang, X. Sun, W. Mao, W. Sun, J. Tang, M. Sui, Y. Shen and Z. Gu, Tumor Redox Heterogeneity-Responsive Prodrug Nanocapsules for Cancer Chemotherapy, *Adv. Mater.*, 2013, **25**(27), 3670–3676.

40 I. S. Alferiev, R. Iyer, J. L. Croucher, R. F. Adamo, K. Zhang, J. L. Mangino, V. Kolla, I. Fishbein, G. M. Brodeur, R. J. Levy and M. Chorny, Nanoparticle-mediated delivery of a rapidly activatable prodrug of SN-38 for neuroblastoma therapy, *Biomaterials*, 2015, **51**, 22–29.

41 X. Liu, Q. Huang, C. Yang, Q. Zhang, W. Chen, Y. Shen and M. Sui, A multi-stimuli responsive nanoparticulate SN38 prodrug for cancer chemotherapy, *J. Mater. Chem. B*, 2017, **5**(4), 661–670.

42 G. Cheng, X. Zhang, Y. Chen, R. J. Lee, J. Wang, J. Yao, Y. Zhang, C. Zhang, K. Wang and B. Yu, Anticancer activity of polymeric nanoparticles containing linoleic acid-SN38 (LA-SN38) conjugate in a murine model of colorectal cancer, *Colloids Surf., B*, 2019, **181**, 822–829.

43 K. Huang, S. Xie, W. Wang, Z.-S. Wu, J. Wu, L. Jiang, J. Chen and J. Li, A hydrogen sulfide-responsive prodrug for monitoring real-time release and improving therapeutic effects of anticancer drug SN-38, *Sens. Actuators, B*, 2022, **373**, 132750.

44 H. Wang, Q. Lu, Y. Miao, J. Song, M. Zhang, Z. Wang, H. Zhang, Z. He, C. Tian and J. Sun, Boosting SN38-based oral chemotherapy to combine reduction-bioactivated structured lipid-mimetic prodrug with ascorbic acid, *Nano Res.*, 2022, **15**(10), 9092–9104.

45 C. Lee, W. Yang and R. G. Parr, Development of the Colle-Salvetti correlation-energy formula into a functional of the electron density, *Phys. Rev. B: Condens. Matter Mater. Phys.*, 1988, **37**(2), 785–789.

46 M. Elayyan, B. Sui and M. R. Hoffmann, Perspective on the Role of Quantum Mechanical Calculations on Cellular Molecular Interactions, *Frontiers in Computational Chemistry*, Bentham Science Publishers, 2024, vol. 7, pp 78–155.

47 S. Grimme, J. Antony, S. Ehrlich and H. Krieg, A consistent and accurate ab initio parametrization of density functional dispersion correction (DFT-D) for the 94 elements H-Pu, *J. Chem. Phys.*, 2010, **132**(15), 154104.

48 S. Grimme, S. Ehrlich and L. Goerigk, Effect of the damping function in dispersion corrected density functional theory, *J. Comput. Chem.*, 2011, **32**(7), 1456–1465.

49 W. J. Hehre, R. Ditchfield and J. A. Pople, Self—Consistent Molecular Orbital Methods. XII. Further Extensions of Gaussian—Type Basis Sets for Use in Molecular Orbital Studies of Organic Molecules, *J. Chem. Phys.*, 1972, **56**(5), 2257–2261.

50 V. A. Rassolov, J. A. Pople, M. A. Ratner and T. L. Windus, 6-31G* basis set for atoms K through Zn, *J. Chem. Phys.*, 1998, **109**(4), 1223–1229.

51 C. A. Hunter and J. K. M. Sanders, The nature of.pi.-.pi. interactions, *J. Am. Chem. Soc.*, 1990, **112**(14), 5525–5534.

52 C. R. Martinez and B. L. Iverson, Rethinking the term ''pi-stacking'', *Chem. Sci.*, 2012, **3**(7), 2191–2201.

53 Y. Zhang, W. Zhao, Y. Chen, H. Yuan, H. Fang, S. Yao, C. Zhang, H. Xu, N. Li, Z. Liu, Z. Guo, Q. Zhao, Y. Liang and W. He, Rational construction of a reversible arylazo-based NIR probe for cycling hypoxia imaging in vivo, *Nat. Commun.*, 2021, **12**(1), 2772.

